Bull. Mater. Sci., Vol. 20, No. 6, September 1997, pp. 845–878. © Printed in India.

Monte Carlo and molecular dynamics simulation of argon clusters and *n*-alkanes in the confined regions of zeolites†

CHITRA RAJAPPA, SANJOY BANDYOPADHYAY and YASHONATH SUBRAMANIAN*‡

Solid State and Structural Chemistry Unit, ‡Also at Supercomputer Education and Research Centre, Indian Institute of Science, Bangalore 560 012, India

Abstract. Geometry and energy of argon clusters confined in zeolite NaCaA are compared with those of free clusters. Results indicate the possible existence of magic numbers among the confined clusters. Spectra obtained from instantaneous normal mode analysis of free and confined clusters give a larger percentage of imaginary frequencies for the latter indicating that the confined cluster atoms populate the saddle points of the potential energy surface significantly. The variation of the percentage of imaginary frequencies with temperature during melting is akin to the variation of other properties. It is shown that confined clusters might exhibit inverse surface melting, unlike medium-to-large-sized free clusters that exhibit surface melting. Configurational-bias Monte Carlo (CBMC) simulations of *n*-alkanes in zeolites Y and A are reported. CBMC method gives reliable estimates of the properties relating to the conformation of molecules. Changes in the conformational properties of *n*-butane and other longer *n*-alkanes such as *n*-hexane and *n*-heptane when they are confined in different zeolites are presented. The changes in the conformational properties of *n*-butane and *n*-hexane with temperature and concentration is discussed. In general, in zeolite Y as well as A, there is significant enhancement of the *gauche* population as compared to the pure unconfined fluid.

Keywords. Argon clusters; *n*-alkanes; zeolites; Monte Carlo; molecular dynamics.

1. Introduction

Clusters exhibit properties different from those of individual atoms or molecules as well as that of bulk. The study of clusters is not only interesting for its own sake but also because it can provide insight into the transition from the individual to the bulk behaviour (Nauchitel and Pertsin 1980; Honeycutt and Andersen 1987; Berry and Cheng 1992). One of the characteristic features of clusters of small sizes (≈ 5–100 atoms or molecules) is that their properties do not vary smoothly with the cluster size, n. Clusters of certain sizes seem to be significantly stabler than the neighbouring sizes — these values of n are termed magic numbers (Hoare and Pal 1970; Frantz 1995). The properties of free clusters get significantly altered when they are confined in a host matrix. The extent to which a specific property will be altered would depend on the nature of the confining medium. Our aim here is to consider two specific, though somewhat unconnected systems: (i) argon clusters confined in zeolites NaCaA and L, and (ii) alkanes (C_4 to C_8 and C_{10}) in zeolites Y and A. We shall see how the properties of free argon clusters such as

†Contribution No. 1260 from the Solid State and Structural Chemistry Unit

*Author for correspondence

structure, energetics, dynamics and melting behaviour are modified when they are confined in zeolitic cages. Instantaneous normal mode analysis (Adams and Stratt 1990a) of the free and confined clusters are also presented.

The study of the adsorption and conformational properties of long chain *n*-alkane molecules in zeolites is relevant to many practical applications and is interesting from a theoretical point of view. A proper investigation of the conformational behaviour of flexible alkane molecules within the zeolite is essential to understand other properties. Many experiments have been attempted to determine the sorption behaviour of alkanes in zeolites (Richards and Rees 1987; Thamm 1987). But it is difficult to obtain experimentally the behaviour of adsorbed molecules at a molecular level. Only recently NMR techniques have been used to study the adsorption and diffusion in zeolites (Chmelka *et al* 1991; Karger and Ruthven 1992). PFG NMR has been used to study the self-diffusion of *n*-alkanes from methane to *n*-heptane in zeolites NaCaA and NaX (Karger *et al* 1980; Heink *et al* 1992). But detailed information on the conformational behaviour of industrially important long-chain *n*-alkanes is not available.

Molecular simulation methods enable one to study the adsorption, diffusion and conformational properties of long chain molecules. These methods have been used by Theodorou and coworkers (June *et al* 1990, 1992) to study the conformations of *n*-butane and *n*-hexane in silicalite at different sorbate loadings. Recently, adsorption of *n*-alkanes, ranging from butane to dodecane has been studied in silicalite and mordenite at zero coverage limit by Smit and Siepmann (1994a). Thermodynamics, conformational and diffusion related properties of *n*-butane and *n*-hexane in silicalite have been studied in detail by Hernandez and Catlow (1995) using molecular dynamics (MD) technique. Recently Theodorou and coworkers (Maginn *et al* 1995) have reported adsorption of *n*-alkanes, ranging from C_4 to C_{25} in silicalite, using a bias MC technique. We shall see how the conformational properties of *n*-alkanes are altered on confinement. Calculations have been performed which attempt to obtain the underlying reasons for these differences.

2. Model

Structural details of the host zeolites as well as details of the potential parameters are given below for studies pertaining to both argon clusters and *n*-alkane molecules in zeolites.

2.1 *Structural details*

We have carried out MC simulations of Ar_6, Ar_7 and Ar_{13} clusters confined to the α-cages in zeolite NaCaA. We have also studied the melting behaviour of an Ar_{13} cluster confined in zeolite L. *n*-alkanes in zeolites Y and A have been investigated.

2.1a *Zeolite NaCaA*: The structure of zeolite NaCaA was taken from the work of Pluth and Smith (1980). Zeolite NaCaA crystallizes in the cubic space group $Fm\bar{3}c$ and has an edge length of 24·555 Å. Each unit cell of zeolite NaCaA contains 192 Si, 384 O, 32 Na and 32 Ca atoms. There are eight large cavities of about

11·4 Å in diameter in every unit cell — these are termed α-cages. Each α-cage is octahedrally connected to six other α-cages via 8-ring windows with diameters ~ 4·5 Å.

2.1b *Zeolite NaY*: Zeolite Y belongs to $Fd\bar{3}m$ space group. The structure was taken from the neutron diffraction studies of Fitch *et al* (1986). The cubic unit cell has an edge length of 24·85 Å and consists of 144 Si, 48 Al, 384 O and 48 Na atoms, corresponding to a Si/Al ratio of 3. The sodium atoms occupy all the SI and SII sites completely and there is zero occupancy of the SIII sites for this ratio of Si/Al and, hence, there is no partial occupancy associated with any of the sites. The network of voids in this zeolite consists of eight α-cages (each of which is ~ 11·8 Å in diameter) in one unit cell. Every α-cage is tetrahedrally interconnected with four other cages via 12-membered rings of approximate diameter 7·4 Å.

2.1c *Zeolite L*: The structure of zeolite L was taken from recent high-resolution neutron powder diffraction studies of Wright *et al* (1985). The zeolite belongs to the *P6/mmm* space group with $a = 18{\cdot}6673$ Å and $c = 7{\cdot}4956$ Å. This zeolite has a structure consisting of channels along the c-direction. Each channel is made up of cage-like units interconnected by 12-membered rings. Consecutive 12-rings are separated by a distance of 7·5 Å along the c-direction. The channel is widest (diameter ~ 13 Å) midway between the two 12-rings.

Figure 1 shows an α-cage in each of zeolites NaCaA and NaY, as well as one of the cage-like units that constitute the channels in zeolite L.

2.2 *Intermolecular potentials*

2.2a *Argon clusters in zeolites*: Interactions between the argon atoms in the cluster was modelled by a simple (6,12) Lennard-Jones potential:

$$\phi(r) = 4\varepsilon\,[(\sigma/r)^{12} - (\sigma/r)^{6}]\,, \tag{1}$$

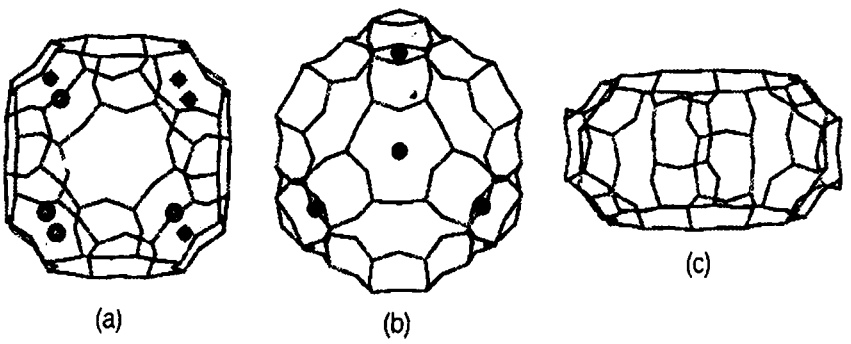

Figure 1. (a) A single α-cage of zeolite NaCaA has been shown. (b) A single α-cage in zeolite NaY is shown. (c) One of the cage-like units that make up the channels in zeolite L is shown in the figure.

where r denotes the interatomic separation. ε and σ are, respectively, the well depth and the diameter of the interacting atoms. In the present calculation, we have taken the values of σ and ε from the work of Davis *et al* (1987).

The total guest–guest interaction energy, i.e. the total interaction between the cluster atoms, is the sum over all such interactions:

$$U_{gg} = \frac{1}{2} \sum_{i=1}^{N} \sum_{j=1,\, j \neq i}^{N} \phi(r_{ij}) = \frac{1}{2} \sum_{i=1}^{N} u_{gg}(r_i), \tag{2}$$

where i and j denote cluster atoms.

The atoms of the cluster also interact with the atoms of the confining zeolite lattice. In the case of a rare-gas cluster confined in zeolite NaCaA, the Ar atoms are assumed to interact only with the O, Na and Ca atoms of the zeolite framework. In the case of Ar_{13}, confined to zeolite L, the cluster atoms interact with the O atoms of the zeolite lattice. In both cases, we neglect the interaction of the cluster atoms with the Si and Al atoms, since they are effectively screened by the bulkier oxygen atoms. These interactions of a cluster atom with a zeolite atom were also taken to be of the (6,12) Lennard-Jones form: $\phi_{iz}(r_{iz})$, where i is a cluster atom and $z = O$ for zeolite L and $z = O$, Na or Ca for zeolite NaCaA. The total cluster–zeolite interaction energy is therefore given by

$$U_{gh} = \sum_{i=1}^{N} \sum_{z} \phi(r_{iz}) = \sum_{i=1}^{N} u_{gh}(r_i). \tag{3}$$

The self-interaction parameters for the zeolite atoms in NaCaA were taken from Kiselev and Du (1981) and from Inglesfield (1982). For zeolite L, the self-interaction parameters for the O–O interaction have been calculated from the work of Henson *et al* (1993). The cluster atom–zeolite interaction parameters were then calculated using the Lorentz–Berthelot combination rules (Allen and Tildesley 1987).

Both the guest–guest and guest–zeolite potentials were shifted so as to have zero energy at the cut-off radius. The total potential energy of the system is the sum of the contributions from the guest–guest and guest–zeolite interactions,

$$U = U_{gg} + U_{gh}. \tag{4}$$

The potential parameters for all interactions are listed in table 1.

2.2b *n-butane in zeolites*: (i) Intramolecular interactions: Alkane molecules have been modelled in terms of united-atom interaction sites or beads, i.e. methyl (CH_3) and methylene (CH_2) groups are represented as single interaction centres, each with appropriate mass of 15 or 14 g mol^{-1} and the site of interaction coinciding with position of the C atom. The distance between these interaction sites is assumed to be the same as the C–C bond lengths viz. 1·53 Å. This model has been found to be successful in modelling *n*-butanes (Smit and Siepmann 1994a; Hernandez and Catlow 1995; Maginn *et al* 1995). Bond bending interactions between three adjacent sites are modelled in terms of a harmonic potential (Van der Ploeg and Berendsen 1982)

$$\phi_b(\theta) = \frac{1}{2} k_\theta (\theta - \theta_0)^2, \tag{5}$$

where θ_0 is the equilibrium bond angle of 114° and the force constant $k_\theta = 6{\cdot}25 \times 10^4$ K rad^{-2}. A torsional potential, governing rotation about non-terminal bonds is expressed in terms of a model proposed by Jorgensen *et al* (1984)

$$\phi_t(\phi) = a_1(1 + \cos\phi) + a_2(1 + \cos 2\phi) + a_3(1 + \cos 3\phi), \tag{6}$$

with $a_1 = 355{\cdot}03$ K, $a_2 = -68{\cdot}19$ K, $a_3 = -791{\cdot}32$ K. For alkane molecules longer than butane, the sites belonging to the same molecule, which are separated by more than three bonds, interact with each other through (6,12) Lennard-Jones potential

$$\phi_{nb}(r_{ss}^{nb}) = 4\varepsilon_{ss}\left[\left(\frac{\sigma_{ss}}{r_{ss}^{nb}}\right)^{12} - \left(\frac{\sigma_{ss}}{r_{ss}^{nb}}\right)^{6}\right]. \tag{7}$$

Table 1. Potential parameters for guest–guest and guest–zeolite interactions for Ar clusters in zeolites.

Type	σ (Å)	ε (kJ/mol)
Ar–Ar	3·4	1·00568
For clusters confined in zeolite NaCaA:		
Ar–O	3·095	1·33038
Ar–Na	3·33	0·29920
Ar–Ca	3·375	3·09831
For clusters confined in zeolite L:		
Ar–O	2·96785	1·22469

Table 2a. Self-interaction parameters for *n*-alkane molecules.

Type	σ (Å)	ε (K)
CH_3–CH_3	3·93	114
CH_2–CH_2	3·93	47

Table 2b. Potential parameters for sorbate–zeolite interactions for *n*-alkane molecules in zeolites.

Type	A_{sz} (10^3 kJ/mol Å^6)	B_{sz} (10^6 kJ/mol Å^{12})
CH_3–O	5·0898	5·8592
CH_3–Na	1·8230	4·3085
CH_2–O	3·2681	3·7622
CH_2–Na	1·1705	2·7664

The self-interaction parameters of *n*-butane molecules used in the present study were taken from the work of Smit and Siepmann (1994a) and are listed in table 2a. The cross-interaction parameters between CH_3 and CH_2 groups are obtained from the well-known Lorentz-Berthelot combination rules (Allen and Tildesley 1987).

(ii) Intermolecular interactions: The intermolecular site–site interactions between *n*-butane molecules are modelled in terms of united-atom model consisting of site–site pairwise interactions of the (6,12) Lennard-Jones form given by:

$$\phi_{ss}(r_{ss}) = 4\varepsilon_{ss}\left[\left(\frac{\sigma_{ss}}{r_{ss}}\right)^{12} - \left(\frac{\sigma_{ss}}{r_{ss}}\right)^{6}\right]. \tag{8}$$

The parameters used are the same as those listed in table 2a.

(iii) Sorbate–zeolite interactions: The sorbate–zeolite interactions $\phi_{sz}(r_{sz})$ are modelled in terms of pairwise (6,12) Lennard-Jones form

$$\phi_{sz}(r_{sz}) = 4\varepsilon_{sz}\left[\left(\frac{\sigma_{sz}}{r_{sz}}\right)^{12} - \left(\frac{\sigma_{sz}}{r_{sz}}\right)^{6}\right], \tag{9}$$

with interaction parameters σ_{sz} and ε_{sz}, between the united atoms $s = CH_3$ or CH_2 and zeolite atoms $z = O$, Na. Interactions between the sorbate molecule and the framework Si/Al atoms are not included since the close approach of the sorbates is prevented by the surrounding bulkier oxygens. The self-interaction parameters of the zeolite atoms used in this study are $\sigma_O = 2{\cdot}545$ Å, $\sigma_{Na} = 3{\cdot}37$ Å, $\varepsilon_O = 155{\cdot}1$ K, $\varepsilon_{Na} = 4{\cdot}72$ K (Santikary *et al* 1992). The cross-interaction parameters between *n*-butane and the zeolite atoms are obtained by the use of combination rules (Allen and Tildesley 1987) and are listed in table 2b. The dispersion and the repulsive interaction terms between the sorbate and the zeolite atom are given by $A_{sz} = 4\varepsilon_{sz}\sigma_{sz}^6$ and $B_{sz} = 4\varepsilon_{sz}\sigma_{sz}^{12}$ respectively.

The total potential energy of interaction U_{tot} is obtained from each of the above-mentioned interactions by summing over the contributions from individual molecules and their mutual interactions and interactions with the zeolite atoms. Therefore, for a system with N alkane molecules each with M sites the total bond-bending interaction energy, U_b, is the sum over all bond-bending interactions:

$$U_b = \sum_{i=1}^{N}\sum_{j=1}^{M-2}\phi_b(\theta_{ij}). \tag{10}$$

The total torsional interaction energy, U_t, is the sum over all torsional interactions:

$$U_t = \sum_{i=1}^{N} \sum_{j=1}^{M-3} \phi_t(\phi_{ij}) . \tag{11}$$

The total intramolecular non-bonded interaction energy, U_{nb}, is obtained by summing the interaction between the sites of the same molecule separated by more than three bonds:

$$U_{nb} = \sum_{i=1}^{N} \sum_{j=1}^{M-4} \sum_{k=j+4}^{M} \phi_{nb}(r_{ijk}) . \tag{12}$$

The total intermolecular interaction energy, U_{ss}, between two different alkane molecules is the sum over all site–site interactions:

$$U_{ss} = \frac{1}{2} \sum_{i=1}^{N} \sum_{j \neq i}^{N} \sum_{k=1}^{M} \sum_{l=1}^{M} \phi_{ss}(r_{ijkl}) . \tag{13}$$

The total alkane–zeolite interaction energy, U_{sz}, is the sum over interactions between the sites of the alkane molecules with all zeolite atoms (N_z):

$$U_{sz} = \sum_{i=1}^{N} \sum_{j=1}^{M} \sum_{k=1}^{N_z} \phi_{sz}(r_{ijk}) . \tag{14}$$

The total potential energy of interaction is therefore given by

$$U_{tot} = U_b + U_t + U_{nb} + U_{ss} + U_{sz} . \tag{15}$$

Note that for *n*-butane $U_{nb} = 0$.

2.3 *Configurational-bias Monte Carlo (CBMC) for alkanes*

Before describing the configurational-bias Monte Carlo (CBMC) method, it would be worthwhile to discuss the usefulness and limitations of the conventional Monte Carlo (MC) technique. In a typical MC move, a particle is moved to an arbitrary position. Therefore, in a MC simulation one does not have to follow the 'natural path' of the particles. This is a significant advantage of MC simulation techniques over molecular dynamics (MD), particularly for systems where diffusion is slow, and, consequently, a very long MD run is essential to obtain reliable results. The conventional MC technique is an efficient method for systems consisting of small molecules, but it fails to work for complex systems such as long chain alkanes, polymers, biomolecules etc. For example, random insertions of long flexible alkanes within the highly ordered and confining environment of the intracrystalline pores of zeolites have a very low probability of success due to very high probability of overlap with the zeolitic walls. To illustrate, the probability for a successful move of a small methane molecule within a zeolite is approximately 10^{-3}, for ethane this is of the order of 10^{-6}, and for longer alkanes this probability is so small that

almost none of the attempted moves will be accepted. This problem can be overcome by using biased insertions instead of random ones. A number of MC techniques have appeared in literature in recent years which utilize biased chain insertions (Harris and Rice 1988; Frenkel *et al* 1992; de Pablo *et al* 1992, 1993; Siepmann and Frenkel 1992; Siepmann *et al* 1993a). This class of simulation methods are known as 'configurational-bias Monte Carlo' or CBMC. All these techniques are based on the basic idea of Rosenbluth and Rosenbluth (1955) and involve 'growing' of alkane chains atom-by-atom instead of a random insertion, with a particular bias function that preferentially samples low-energy conformations. The bias introduced while growing a chain molecule is exactly removed by adjusting the acceptance rules (Harris and Rice 1988; Frenkel *et al* 1992; Siepmann and Frenkel 1992). The CBMC techniques have been found to be very efficient in simulating various systems such as *n*-alkanes (Laso *et al* 1992; Siepmann *et al* 1993a, b), phase equilibria of chain molecules (Mooij *et al* 1992) etc. In our work we have employed CBMC technique as proposed by Smit and Siepmann (1994a, b), which is described below.

The underlying idea of this technique is to generate trial conformations of the alkane molecules in a smart way i.e. in such a way that the trial chain avoids overlapping with itself and with other chains in the system and also takes into account the intramolecular potentials. This smart generation of conformations is an efficient way of sampling and it gives rise to high acceptance probability of the attempted moves.

Consider a system with N identical alkane molecules each with M sites. A new conformation of an alkane molecule is generated, using the following steps: Step 1: One alkane molecule and one of its sites are selected randomly. Step 2: The selected alkane molecule is then either completely or partially re-grown depending on the selected site. If the selected site is the first or last bead of the chain then the CBMC move involves discarding the entire molecule and then regrowing it site-by-site. If the selected site is in the interior of the chain, then a random choice is made to decide whether to re-grow the head or the tail part of the chain. Now, suppose a non-terminal site l is chosen. If the tail part is selected, then the sites l to M are re-grown. If the head is selected, then the sites 1 to l are re-grown. This move is very efficient in changing the conformation of an alkane molecule. Now, suppose a non-terminal site l is chosen in a particular move and the tail part of the chain is to be re-grown. This process of re-growing a chain is shown schematically in figure 2. A set of k trial positions is generated as $\{\mathbf{b}\} = (\mathbf{b}_1, \mathbf{b}_2, \ldots, \mathbf{b}_k)$ on the surface of a sphere with $(l-1)$-th atom at the centre of the sphere and the radius equal to the bond length. This set of trial orientations is generated using the internal part of the potential (i.e. only the bond–bonding and torsional interactions), which results in the following distribution for the lth atom

$$p_l^{\text{int}}(\mathbf{b}_i)\, \mathrm{d}\mathbf{b}_i = \frac{\exp\left[-\beta\, u_l^{\text{n. int}}(\mathbf{b}_i)\right]\, \mathrm{d}\mathbf{b}_i}{C}, \tag{16}$$

where $\beta = 1/k_b T$ and C is a normalization constant given by

$$C \equiv \int_b \exp\left[-\beta\, u_l^{\text{n. int}}(\mathbf{b}_i)\right] \mathrm{d}\mathbf{b}_i . \tag{17}$$

In CBMC scheme one does not have to calculate this constant. This internal potential energy $u_l^{\text{n. int}}(\mathbf{b}_j)$ and hence the probability $p_l^{\text{int}}(\mathbf{b}_j)$ depends on which type of atom is being inserted. Of each of these k trial positions the external interaction energy $u_l^{\text{n. ext}}(\mathbf{b}_j)$ is calculated with the atoms of the other alkane molecules and with those of the zeolite and also with those sites of the molecule which are already grown and separated by at least four sites. Then one of these k trial positions is selected with a probability

$$p_l^{\text{ext}}(\mathbf{b}_j) = \frac{\exp\left[-\beta\, u_l^{\text{n. ext}}(\mathbf{b}_j)\right]}{w^{\text{n. ext}}(l)}, \tag{18}$$

where

$$w^{\text{n. ext}}(l) = \sum_{j=1}^{k} \exp\left[-\beta\, u_l^{\text{n. ext}}(\mathbf{b}_j)\right]. \tag{19}$$

This process is repeated until the last site of the chain is reached. When regrowing of the entire alkane chain of length M is complete, one calculates

$$W^{\text{n}} = \prod_{i=1}^{l-1} \exp\left[-\beta\, u^{\text{n. ext}}(i)\right] \prod_{j=1}^{M} w^{\text{n. ext}}(j). \tag{20}$$

Step 3: After a new conformation of the selected chain has been generated, one proceeds by considering the old configuration of the selected molecule. The external energy $u^{\text{o. ext}}(l)$ is calculated and a set of $(k-1)$ trial orientations is generated. One then calculates,

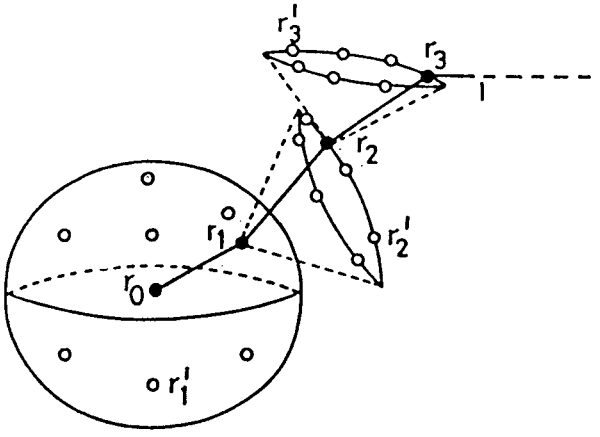

Figure 2. Schematic representation of the CBMC move to efficiently grow conformations of alkanes confined in zeolitic pores. r_0 is the starting position of the chain. r_1, r_2 etc (shown as filled spheres) are the additional atomic positions, which are selected from among a set of trial positions r_i' generated on the surface of a sphere with radius equal to the bond length (shown as empty spheres).

$$w^{o,\,ext}(l) = \exp\left[-\beta\, u^{o,\,ext}(l)\right] + \sum_{j=2}^{k} \exp\left[-\beta\, u^{o,\,ext}(\mathbf{b}_j)\right]. \tag{21}$$

When all the sites of the molecule have been considered, one calculates for the entire molecule

$$W^{o} = \prod_{i=1}^{l-1} \exp\left[-\beta\, u^{o,\,ext}(i)\right] \prod_{j=1}^{M} w^{o,\,ext}(j). \tag{22}$$

Step 4: Finally, whether the new conformation of the alkane molecule will be accepted or not is decided by the acceptance rule

$$\mathrm{acc}(o \rightarrow n) = \min(1,\ W^{n}/W^{o}). \tag{23}$$

This acceptance rule removes the bias of the growing process, obeys detailed balance, and hence the conformations are generated with the correct Boltzmann weight.

2.4 *Computational details*

2.4a *Canonical ensemble Monte Carlo method for clusters*: In this study, we have used the Metropolis algorithm (Metropolis *et al* 1953) to carry out Monte Carlo simulations of argon clusters confined to cavities in zeolites. We have also studied the melting behaviour of an Ar_{13} cluster confined in zeolite L.

The MC simulations in zeolite NaCaA were carried out with a simulation cell that consisted of a single unit cell of the zeolite. For studies of Ar_{13} confined in zeolite L, the simulation cell was made up of $2 \times 2 \times 3$ unit cells. In all cases, the zeolite framework was assumed to be rigid and merely provided an external field.

Every Monte Carlo step consisted of an attempt to displace each cluster atom in turn. Whenever an attempt was such that the distance of the cluster atom from the cluster centre-of-mass (COM) was greater than 4σ, such a move was rejected. Periodic boundary conditions were imposed and the nearest image used in the calculation of both cluster atom–cluster atom, as well as cluster atom–zeolite lattice interactions. A spherical cutoff of 10 Å was used for both guest–guest and guest–zeolite interactions.

At each temperature, the system was equilibrated for 10^6 MC steps. This was followed by a production run of 7×10^6 MC steps. Coordinates of the cluster atoms and the associated energies of interaction were stored every 100 MC steps from which all properties were calculated. The configuration of the cluster at the first step after the equilibration run at a given temperature was used as the starting configuration for the MC run at the next higher temperature.

2.4b *Configurational-bias Monte Carlo for n-alkanes*: Monte Carlo (MC) calculations have been carried out in the canonical ensemble at fixed (N, V, T). Cubic periodic boundary conditions were employed. An attempt is made to displace a molecule randomly, rotate it by a random magnitude around a randomly chosen

axis and, finally, to re-grow either a part or whole of it. N such attempts comprise a MC cycle during which the molecule itself is selected randomly. CBMC method has been employed to re-grow the molecules. Attempt to re-grow the molecules is carried out as proposed by Smit and Siepmann (1994a) and the method is referred to as configurational-bias Monte Carlo (CBMC). The centre-of-mass of the selected molecule is displaced randomly within $\pm 0{\cdot}3$ Å and a maximum rotation of the molecule by $\pm 3°$ is allowed around a randomly chosen axis. During the CBMC move, the number of trial positions, k, generated for each site using the internal part of the potential is 6. One unit cell of zeolites NaY and NaCaA, each consisting of eight α-cages have been employed in the present study. All the simulations have been carried out at a fixed temperature of 400 K with eight n-alkane molecules, corresponding to a sorbate concentration, c, of one n-alkane molecule per α-cage. At the start of the simulation, there was precisely one n-alkane molecule in each of the eight α-cages. For every run, equilibration was carried out over 2500 MC cycles. This is followed by production runs of 10^5 MC cycles to obtain averages of the properties. A spherical cut-off of 12 Å has been employed in evaluating both sorbate–sorbate and sorbate–zeolite interaction energies.

3. Results and discussion

3.1 *Argon clusters in zeolites*

3.1a *Structure and energy*: Clusters of rare gases have been widely investigated in their free state, *viz.* when they are not confined in any medium (Etters and Kaelberer 1977; Nauchitel and Pertsin 1980; Quirke and Sheng 1984; Honeycutt and Andersen 1987; Berry and Cheng 1992; Berry 1994). Before we discuss the properties of clusters confined in zeolites, it may be worthwhile to briefly recollect the properties of free clusters of rare gases. Free rare-gas clusters exhibit interesting structural, energetic and dynamical properties. Clusters of 4–55 atoms assume structures with high symmetry. Thus, for example, a cluster with 4 atoms prefers a tetrahedral, 5 a trigonal bipyramidal, 6 an octahedral, 7 a pentagonal bipyramidal, 13 an icosahedral geometry (see figure 3). It is not uncommon to find clusters confined in host matrices. It is of considerable importance to know how and in what way the behaviour of such clusters would be altered by the confinement. In particular, we would like to address the structural and energetic aspects of confined clusters *vis-a-vis* those of free clusters.

Interaction energies, U_t, for free Ar_n clusters, for $n = 4$, 19 are listed in table 3. In figure 4, we have plotted the difference in the total interaction energies of free Ar clusters:

$$\Delta U = U_n - U_{n-1}, \tag{24}$$

where $U_n = U \cdot n/\varepsilon$ is the total interaction energy for a cluster of size n in dimensionless units. Here U is the total interaction energy per particle of (4) in kJ/mol. It is seen that the curve peaks at certain values of n, indicating that clusters of these sizes are much stabler (see figure 4). In particular, clusters with $n = 7$, 13 and 19 exhibit pronounced peaks, indicating considerable stability as compared to others. These are the magic number sizes for free argon clusters.

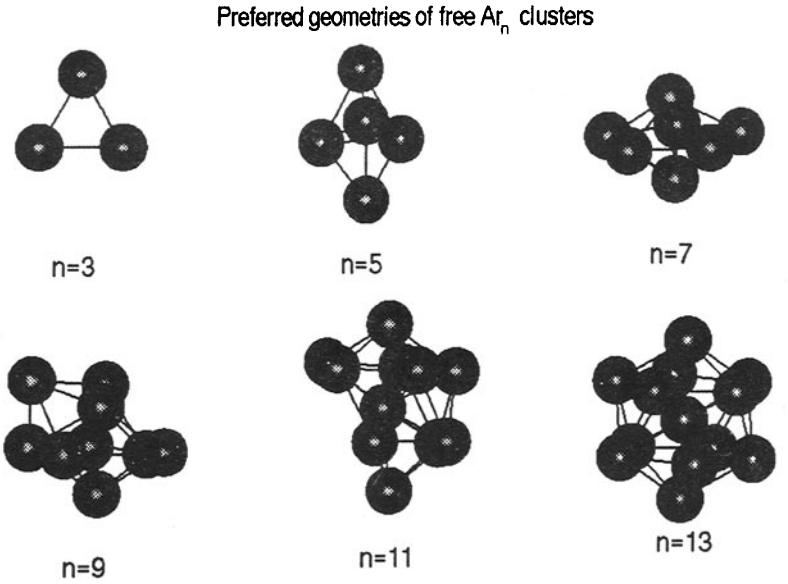

Figure 3. The preferred geometries of some free Ar_n clusters are shown with $4 < n < 19$.

Table 3. The minimum energy configurations obtained for Ar_n, $n = 4$–19 by the process of slow heating have been listed. The temperature at which this minimum energy was observed has been indicated as well as temperature at which the cluster splits.

		Starting configuration			Minimum energy configuration				
Cluster size	U_r (ε)	U_{gg} (kJ/mol)	U_{gh} (kJ/mol)	U (kJ/mol)	U_{gg} (kJ/mol)	U_{gh} (kJ/mol)	U (kJ/mol)	T_1 (K)	T_2 (K)
4	6·0	−0·5059	−1·2623	+0·7563	−17·8414	−1·0083	−16·8332	7	52
5	9·104	−11·2586	−1·6916	−9·5670	−17·7544	−0·8571	−16·8973	7	54
6	12·712	−4·4340	−1·7296	−2·7044	−18·1467	−1·5466	−16·6002	47	55
7	16·505	−9·6940	−2·3179	−7·3761	−18·4552	−1·8057	−16·6495	26	70
8	19·822	+27·1676	−1·5252	+28·9300	−18·2527	−1·7175	−16·5352	53	56
9	24·113	−9·0494	−2·1082	−7·0313	−18·3671	−1·8806	−16·4865	49	62
10	28·420	+0·9451	−1·7636	+2·7088	−17·9856	−1·8537	−16·1319	40	59
11	32·765	+28·2497	−1·5216	+29·7714	−18·0676	−2·1053	−15·9623	6	50
12	37·967	−9·2615	−3·1403	−6·1212	−17·9876	−2·0139	−15·9737	58	60
13	44·327	+10·7191	−3·3911	+14·1102	−17·9057	−2·2551	−15·6507	67	68
14	47·845	+17·4699	−1·1480	+18·6179	−18·3353	−2·3279	−16·0074	63	64
15	52·323	−4·1057	−1·4572	−2·6485	−18·3294	−2·5558	−15·7737	6	75
16	56·816	−4·1249	−1·5721	−2·5528	−18·0851	−3·2009	−14·8841	46	61
17	61·318	+10·7135	−1·6462	+12·3596	−18·1718	−3·1942	−14·9776	7	67
18	66·531	+25·0924	−0·7178	+25·8102	−18·5599	−2·9552	−15·6047	6	78
19	72·660	+6·0538	−1·4230	+7·4767	−18·4711	−3·5066	−14·9645	6	86

T_1: Temperature at which minimum energy configuration is observed; T_2: temperature at which the cluster splits.

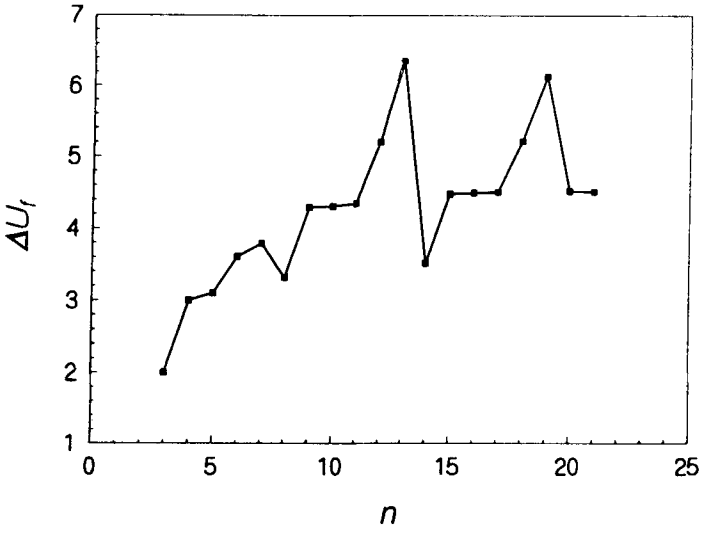

Figure 4. The differences in the binding energies are shown as a function of cluster size for free Ar_n clusters. The peaks in the curve correspond to the so-called magic number cluster sizes: 7, 13 and 19.

There have been a few studies on rare-gas clusters confined in host matrices (Li and Berry 1995a, b). It is not clear from these whether magic number clusters exist among rare-gas clusters confined in zeolites or other host matrices. We have carried out a detailed calculation in which we have studied the structure and the energies associated with Ar_n clusters confined in the α-cages of the host matrix, zeolite NaCaA, for n varying between 4 and 19. Specifically, the clusters were present in the α-cages of zeolite NaCaA. In order to obtain the structure corresponding to the lowest energy minimum, we tried to locate the minimum in the total energy comprising the argon–argon and argon–zeolite interaction energies. This was attempted by carrying out Monte Carlo runs at temperatures starting from 5 K up to the temperature at which the cluster splits in steps of 1 K. This slow heating of the cluster was performed, starting from an arbitrary configuration of the cluster. At low temperatures, the cluster atoms are not very mobile. However, around the melting temperature, we expect that the cluster atoms will be able to sample much more of phase space — they will perhaps be able to overcome barriers that separate local minima from the global minimum. And so, the global minimum is likely to be sampled when the temperature is high enough for the cluster atoms to sample phase space efficiently, but low enough for the cluster to remain a single integrated unit (i.e. without splitting up into smaller sub-clusters) provided that sufficient time is available for the cluster to sample all of the phase space accessible to it at that temperature. For this purpose we have carried out the simulation for a duration of 5000 MC steps at every temperature. To ensure that we have found low-enough energy minima, the procedure is repeated starting from two different initial configurations. The minimum energy is taken to be the lowest of all energies over all MC steps and all temperatures.

Normally, global optimization is performed using the method of simulated annealing

(Kirkpatrick *et al* 1983) where the system temperature is brought down sufficiently slowly. The method employed by us here does exactly the opposite: the temperature is slowly increased until the system samples the configuration space effectively and manages to reach the minimum.

Table 3 lists the energy of the starting configuration, the lowest energy obtained, the temperature at which minimum energy was located and the temperature at which the cluster splits. The individual contributions of the guest–guest and the guest–host interactions have also been listed. It is evident from table 3 that different starting configurations lead to energies which differ at most by 3·6% of each other. Figure 5 shows a plot of ΔU_n, $\Delta U_{n,\mathrm{gg}}$, as well as $\Delta U_{n,\mathrm{gh}}$ as a function of n. As the predominant term is the guest–host interaction term, the behaviour of ΔU_n and $\Delta U_{n,\mathrm{gh}}$ are similar. The curve peaks at several values of n. In particular, $n = 14$ and 18 show pronounced peaks, suggesting the possible existence of magic numbers in argon clusters confined in zeolite NaCaA. However, it is necessary to obtain other properties of these clusters, such as the melting behaviour, before it can be said unambiguously that these cluster sizes are magic numbers for confined clusters in zeolite NaCaA. Also, it is important that a more exhaustive search for the minimum energy is carried out. The structures corresponding to the minimum energies for confined clusters of various sizes (listed in table 3) are displayed in figure 6. The precise geometry of the cluster would depend on the symmetry of the confining medium and the interactions between the medium and the guest. The minimum energy structures for the clusters would be determined by the combination of the guest–guest and the guest–host potential energy surface, and is, therefore, more complex and is not predicted easily. There often exists more than one structure with little difference in energies.

3.1b *Instantaneous normal mode spectra for rare-gas clusters*: Instantaneous normal mode (INM) analysis was originally proposed by Seeley and Keyes (1989) for liquids in order to obtain dynamical properties from a series of configurations obtained either from Monte Carlo or from molecular dynamics simulations and from any ensemble. Normally, one would have to obtain dynamical quantities of interest from simulations that have been carried out in the micro-canonical (NVE) ensemble, using molecular dynamics. Subsequently, Adams and coworkers (1990a) employed INM to study properties of free rare-gas clusters during the process of melting. Attempts to obtain values of diffusion coefficients and other dynamical properties from INM have met with limited success (Adams and Stratt 1990b, c; Beck and Marchioro 1990). There are, however, certain insights that could be gained from INM by the calculation of quantities such as the percentage of imaginary frequencies. Monte Carlo simulations indicate that a free Ar_{13} cluster when heated exhibits a rigid–nonrigid transition from a solid-like to a liquid-like transition around 26 K. We refer to this as the melting temperature. δ, the average mean squared pair distance fluctuation, is defined as

$$\delta = \frac{2}{N(N-1)} \sum_{i<j} \frac{(\langle r_{ij}^2 \rangle - \langle r_{ij} \rangle^2)^{1/2}}{\langle r_{ij} \rangle}, \tag{25}$$

here r_{ij} are the distances between any two cluster atoms and $\langle\ \rangle$ implies averaging

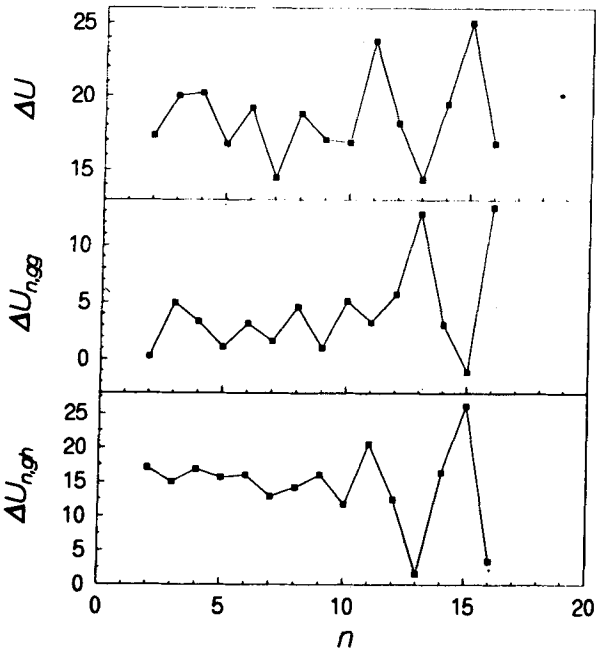

Figure 5. The differences in the binding energies are shown as a function of cluster size for Ar_n clusters confined to the α-cages in zeolite NaCaA.

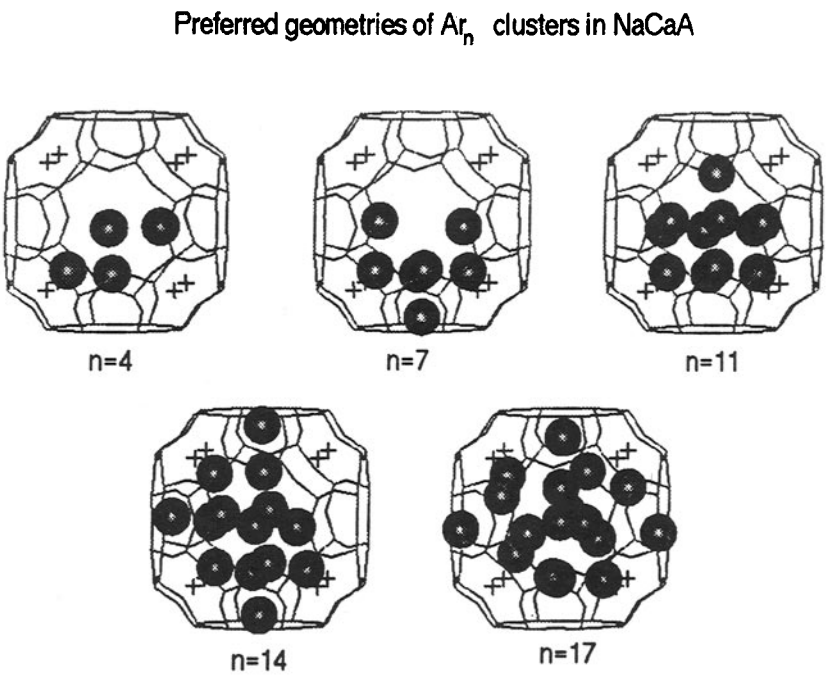

Figure 6. The preferred geometries of some Ar_n clusters confined in zeolite NaCaA are shown, where $4 < n < 19$.

over the entire run. This quantity is usually used to monitor the melting of clusters. The behaviour of δ with temperature for a free Ar_{13} cluster is shown in figure 7. INM spectra were calculated using about 200 MC configurations at different temperatures. Figure 8 shows the INM spectra for the free Ar_{13} cluster at various temperatures. Here the imaginary frequencies are plotted on the negative x-axis. At every temperature two peaks are observed in the spectra, one at a real frequency and another at an imaginary frequency. At low enough temperatures, a high-frequency peak is observed near 60 cm^{-1}, which is characteristic of solid or bulk argon. Thus, in some sense, the central atom of the icosahedral cluster is in a bulk-like environment at low temperatures where it is completely surrounded by the other twelve argon atoms. With increase in temperature, the peak at 60 cm^{-1} disappears as the atoms acquire higher mobility. Also, the area under the imaginary peak increases with temperature, indicating, thereby, that at higher temperatures, the cluster atoms spend more time at the saddle points of the potential energy surface. Thus, the percentage of imaginary frequencies could be a good indicator of the mobility of the cluster atoms. We therefore plot the percentage of imaginary frequencies as a function of temperature in figure 9. The percentage increases with temperature, but exhibits no sharp change at the melting temperature.

We shall now look at the melting behaviour of rare-gas clusters when they are confined in the cages and cavities of zeolites. Table 4 shows the variation of guest–guest, guest–zeolite and the total interaction energies with temperature for the Ar_{13} cluster confined in zeolite NaCaA. Figure 10 shows the variation of δ with temperature for Ar_{13} cluster confined in the cavities of zeolite NaCaA. The starting configuration had an energy of $-18{\cdot}011$ kJ/mol. This energy seems to be the minimum energy for an Ar_{13} cluster confined in an α-cage of zeolite NaCaA.

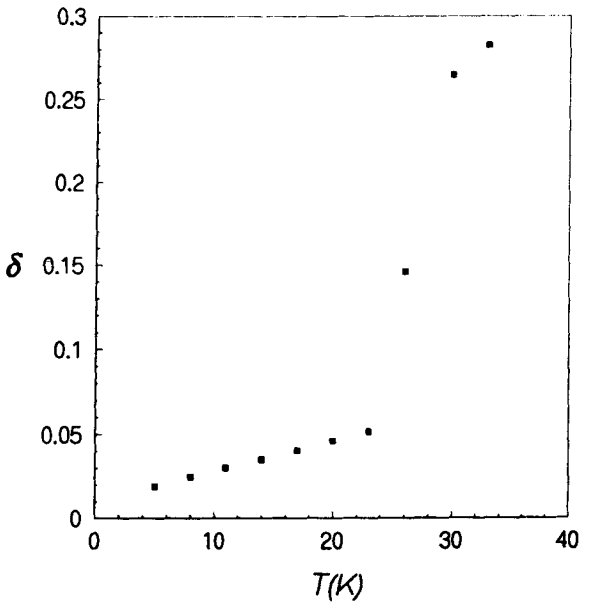

Figure 7. A plot of the root mean squared pair distance fluctuations, δ, has been shown as a function of temperature for a free Ar_{13}.

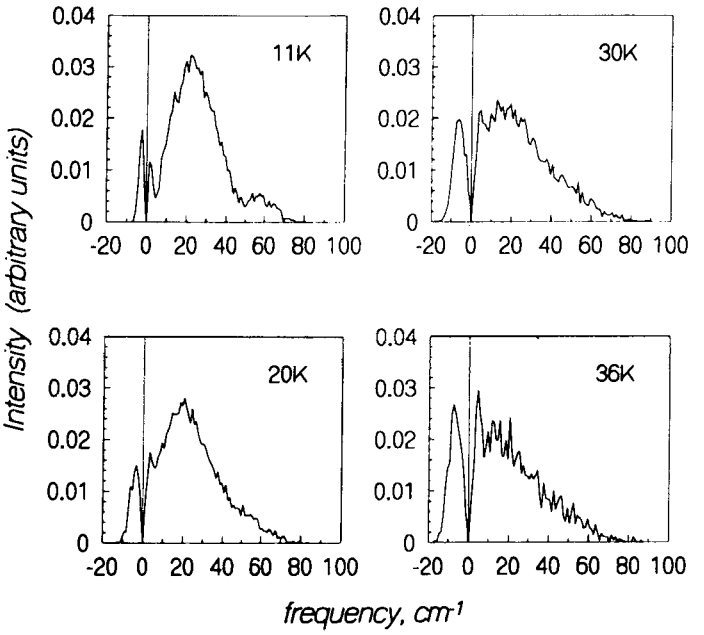

Figure 8. The instantaneous normal mode (INM) spectra are shown for a free Ar_{13} cluster at various temperatures.

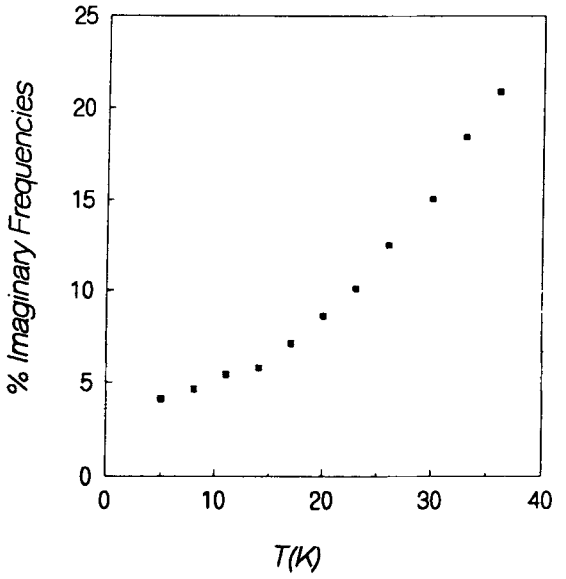

Figure 9. The percentage of imaginary frequencies has been plotted as a function of temperature for a free Ar_{13} cluster.

The melting transition does not appear to be a sharp transition as seen from the figure. The INM spectra were calculated at various temperatures and these are shown in figure 11. The INM spectra were calculated from 1400 MC configurations by selecting every fifth configuration from 7000 MC steps. Again, it is seen that like in the free cluster, there are two peaks at every temperature, one at an imaginary frequency and another at a real frequency. Further, it is seen that the peak at the imaginary frequency increases in intensity with temperature. This suggests that the cluster atoms spend increasing amounts of time at the saddle points of the potential energy surface. Figure 12 shows the dependence of the percentage of imaginary frequencies on the temperature. The variation is similar to the variation of δ with temperature (see figure 10): no sudden transition is found. A few differences with the results for the free cluster are noteworthy: the guest–zeolite interaction energy essentially dominates the properties of the cluster; the percentage of imaginary frequencies at any temperature for the free cluster is usually lower than that for the confined cluster. This suggests that the confined cluster spends a larger fraction of time on the saddle points in the potential energy surface as compared to the free cluster.

Earlier work on Ar_{13} cluster in the zeolite L has shown that such a cluster will exhibit the phenomenon of inverse surface melting: the inner atoms of the confined Ar_{13} cluster melt (acquire mobility) even before the outer atoms melt (Chitra and Yashonath 1997). This is in contrast to the surface melting behaviour exhibited by free clusters of medium to large size, where atoms on the outer surface usually melt before the inner core acquires mobility (Cheng and Berry 1992; Kunz and Berry 1993). INM spectra of the Ar_{13} cluster confined in zeolite L are shown in figure 13 for various temperatures. Each spectrum has been obtained by averaging over about 200 MC configurations. Figure 14 shows the INM spectra for a free Ar_{13} cluster and also for an Ar_{13} cluster confined in zeolite L for a temperature of 5 K. Figure 15 shows the variation of the percentage of imaginary frequencies and the total interaction energy with temperature. It is seen that they both exhibit a similar variation. The changes in the percentage of imaginary frequencies and U are seen to be maximum near the melting temperature, which is ≈ 20 K when the

Table 4. Guest–guest and guest–zeolite interaction energies at various temperatures for Ar_{13} confined in zeolite NaCaA.

T (K)	$\langle U_{gg} \rangle$ (kJ/mol)	$\langle U_{gh} \rangle$ (kJ/mol)
5·0	−2·28938	−15·8354
8·0	−2·28004	−15·8075
11·0	−2·27063	−15·7794
14·0	−2·26117	−15·7514
17·0	−2·25157	−15·7240
20·0	−2·24162	−15·6965
23·0	−2·23193	−15·6692
26·0	−2·22156	−15·6420
29·0	−2·21137	−15·6141
32·0	−2·20084	−15·5869
35·0	−2·19043	−15·5597
38·0	−2·17948	−15·5324

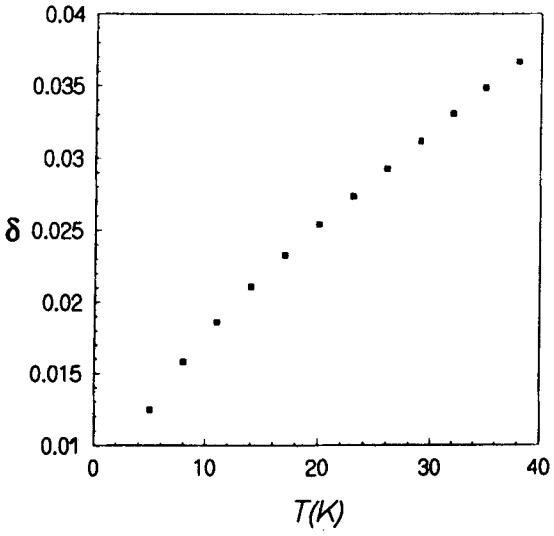

Figure 10. The root mean squared pair distance fluctuation, δ, has been plotted at various temperatures for an Ar_{13} cluster confined in zeolite NaCaA.

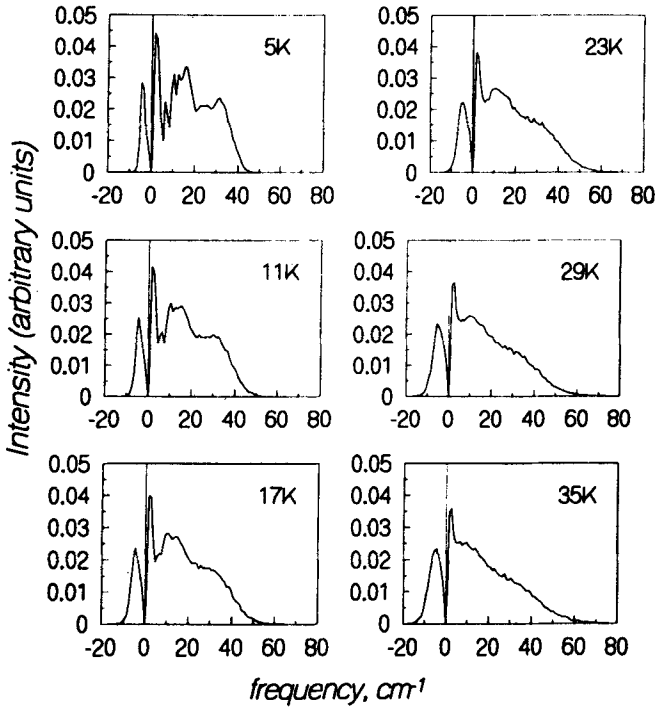

Figure 11. The instantaneous normal mode (INM) spectra are shown at different temperatures for an Ar_{13} cluster confined in zeolite NaCaA.

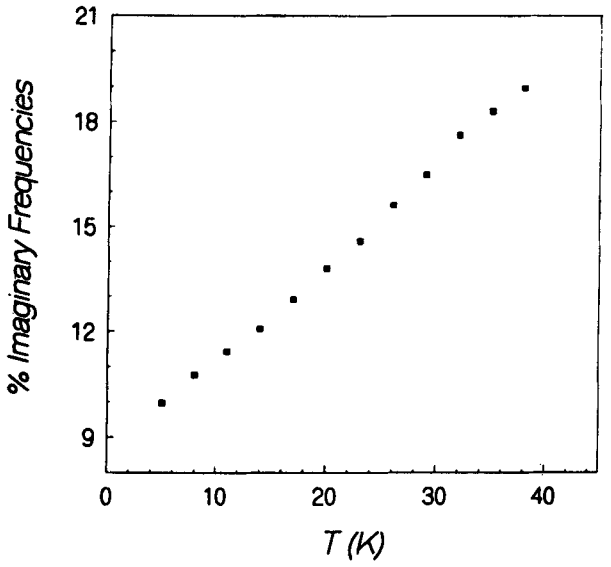

Figure 12. The percentage of imaginary frequencies has been plotted at various temperatures for an Ar_{13} confined in zeolite NaCaA.

inner rare-gas atoms exhibit increased mobility. This is evident from figure 16 which shows the trajectories of each of the 13 argon atoms.

3.2 *n-Alkanes in zeolites*

3.2a *Thermodynamic properties*: The average values of different interaction energies, such as, U_{ss}, U_{sz}, U_{nb}, U_b, U_t and U_{tot} as well as the isosteric heats of adsorption (q_{st}) for different *n*-alkanes (C_4H_{10} to $C_{10}H_{22}$) adsorbed in zeolites NaY and NaCaA are listed in tables 5 and 6, respectively. From the tables it is clear that irrespective of the chain length, M, of the molecules, the alkane–zeolite or sorbate–zeolite interaction energy (U_{sz}), is the predominant one. Contributions from bond-bending interactions (U_b) and torsional interactions (U_t) are almost constant and rather small. The increase in alkane–zeolite or sorbate–zeolite interaction energy (U_{sz}) with increase in chain length is more significant in zeolite NaCaA.

3.2b *n-Alkane conformation*: Figures 17 and 18 display distribution of the dihedral angles, $f(\phi)$, for *n*-alkanes, ranging from *n*-butane (C_4H_{10}) to *n*-decane ($C_{10}H_{22}$) confined in zeolites NaY and NaCaA respectively.

From these plots it is clear that there is no significant population of C–C dihedral bonds in the region between *trans* and *gauche* conformations. Average relative population of *trans* and *gauche* bonds for different *n*-alkanes confined in zeolites NaY and NaCaA are listed in tables 7 and 8, respectively.

It is clear from tables 7 and 8 that, average population of a *gauche* bond is higher for long alkanes ($M \geq 6$) confined in zeolite NaCaA, compared to that in zeolite NaY.

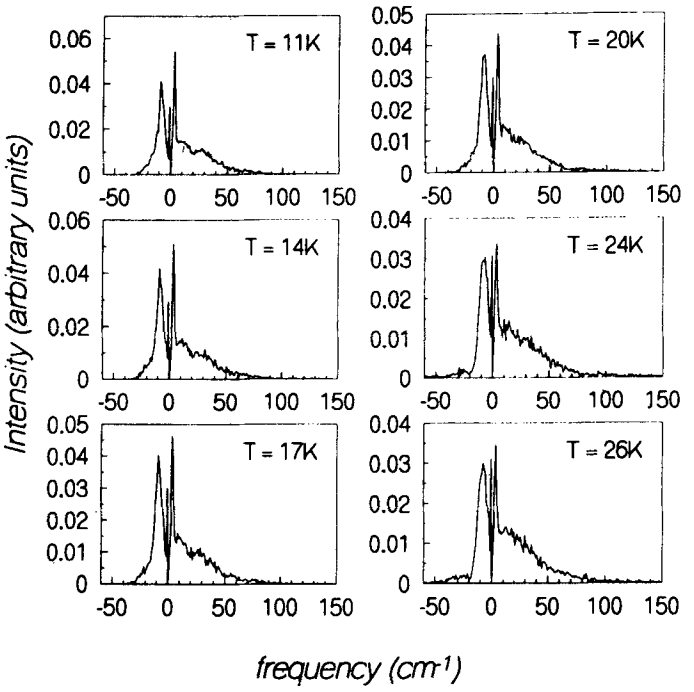

Figure 13. The instantaneous normal model (INM) spectra are shown at different temperatures for an Ar_{13} in zeolite L.

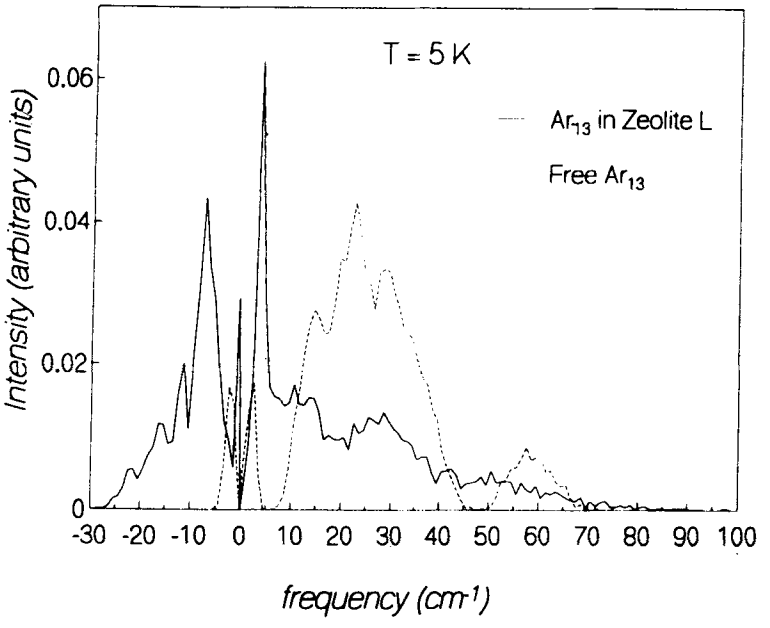

Figure 14. The instantaneous normal model (INM) spectra for a free Ar_{13} cluster (- - -), and an Ar_{13} cluster in zeolite L at 5 K (—).

To investigate the effect of confinement on long *n*-alkanes ($M \geq 6$) in a more detailed way, we have studied the conformation of every individual C–C dihedral bond along the chain. Figure 19 schematically shows the convention that we have adopted in numbering the C–C dihedral bonds.

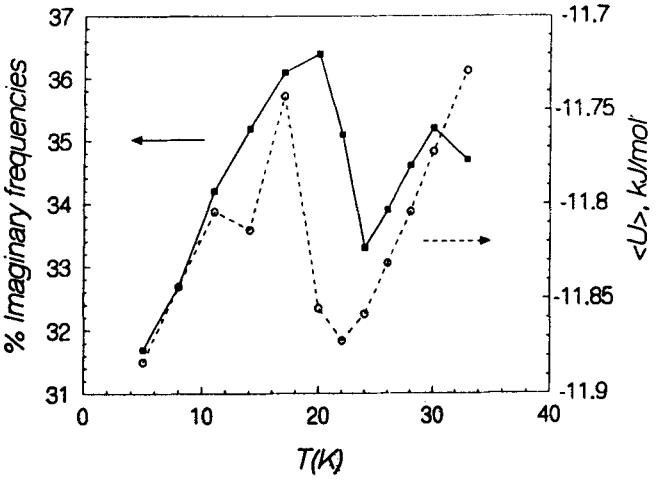

Figure 15. The variation of the total interaction energy, U_{tot}, as well as the percentage of imaginary frequencies with temperature is shown for an Ar_{13} cluster in zeolite L.

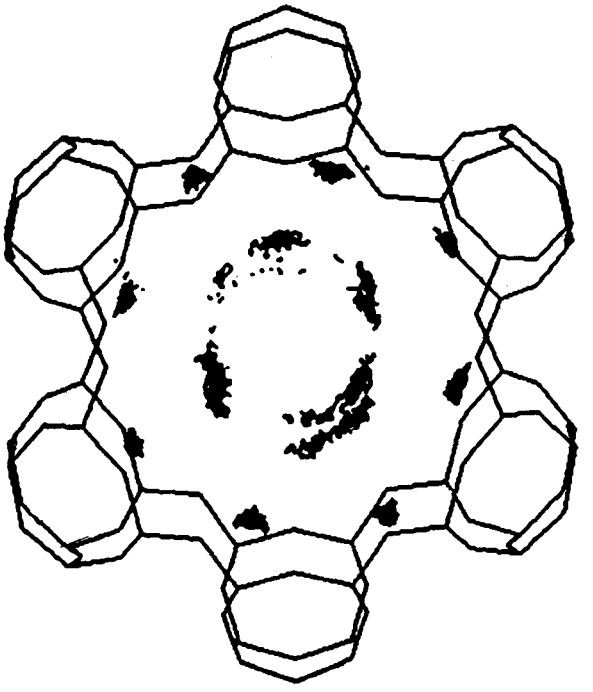

Figure 16. The trajectories of each of the thirteen argon atoms of an Ar_{13} cluster in zeolite L at 24 K have been shown.

There are odd number of C–C dihedral bonds present in hexane, octane and decane (3, 5 and 7 respectively). For these three chains the central C–C dihedral bond is numbered as 1. The other dihedral bonds towards the right of the central bond are numbered in an increasing order (2, 3, ... etc). The bonds which are on the left of the central bond are once again numbered in an increasing order with primes (2′, 3′, ... etc). By symmetry the primed C–C dihedral bonds are identical to the non-primed ones (i.e. $2 \equiv 2'$, $3 \equiv 3'$ etc). There are four C–C dihedral bonds in heptane. We have numbered the two central C–C dihedral bonds as 1 and 1′ and the two terminal dihedral bonds as 2 and 2′ respectively. The *trans* and *gauche* populations of these bonds are listed in tables 9 and 10 for *n*-hexane to *n*-decane confined in zeolites Y and A respectively.

For clarity, the data presented in these tables are shown in figures 20 and 21 for zeolites Y and A respectively.

It is clear from figures 20 and 21 that there exists a pattern in the variation of *gauche* conformer population as one traverses from chain centre towards the chain end across the *n*-alkane series investigated here. It is observed that for *n*-hexane ($M = 6$) and *n*-heptane ($M = 7$) confined in both zeolites Y and A, the probability of a terminal C–C dihedral bond to remain in *gauche* form is higher than the non-terminal C–C dihedral bonds. But from $M > 7$ onwards (*n*-octane and *n*-decane) the trend observed in both the zeolites is different from that observed for smaller

Table 5. Equilibrium thermodynamic properties of *n*-alkanes (C_4H_{10}–$C_{10}H_{22}$) in zeolite NaY at a temperature of 400 K and sorbate concentration, $c = 1$ *n*-alkane/α-cage.

Molecule	U_{ss} (kJ/mol)	U_{sz} (kJ/mol)	U_{nb} (kJ/mol)	U_b (kJ/mol)	U_t (kJ/mol)	U_{tot} (kJ/mol)	q_{st} (kJ/mol)
C_4H_{10}	−1·96	−22·43	–	1·66	3·49	−19·24	22·57
C_5H_{12}	−2·76	−26·91	−0·72	1·65	3·16	−25·58	28·91
C_6H_{14}	−3·69	−31·76	−0·89	1·64	3·19	−31·51	34·84
C_7H_{16}	−4·56	−36·30	−1·13	1·66	3·24	−37·09	40·42
C_8H_{18}	−5·22	−40·26	−1·36	1·66	3·24	−41·94	45·27
$C_{10}H_{22}$	−7·00	−48·77	−1·84	1·66	3·22	−52·73	56·06

Table 6. Equilibrium thermodynamic properties of *n*-alkanes (C_4H_{10}–$C_{10}H_{22}$) in zeolite NaCaA at a temperature of 400 K and sorbate concentration, $c = 1$ *n*-alkane/α-cage.

Molecule	U_{ss} (kJ/mol)	U_{sz} (kJ/mol)	U_{nb} (kJ/mol)	U_b (kJ/mol)	U_t (kJ/mol)	U_{tot} (kJ/mol)	q_{st} (kJ/mol)
C_4H_{10}	−1·45	−51·24	–	1·65	3·41	−47·63	50·96
C_5H_{12}	−2·46	−61·40	−0·73	1·65	3·08	−59·86	63·19
C_6H_{14}	−3·01	−71·86	−0·90	1·65	3·23	−70·89	74·22
C_7H_{16}	−2·39	−81·43	−1·07	1·66	3·53	−79·70	83·03
C_8H_{18}	−3·20	−90·48	−1·08	1·68	3·62	−89·46	92·79
$C_{10}H_{22}$	−6·68	−111·39	−1·41	1·67	3·53	−114·28	117·61

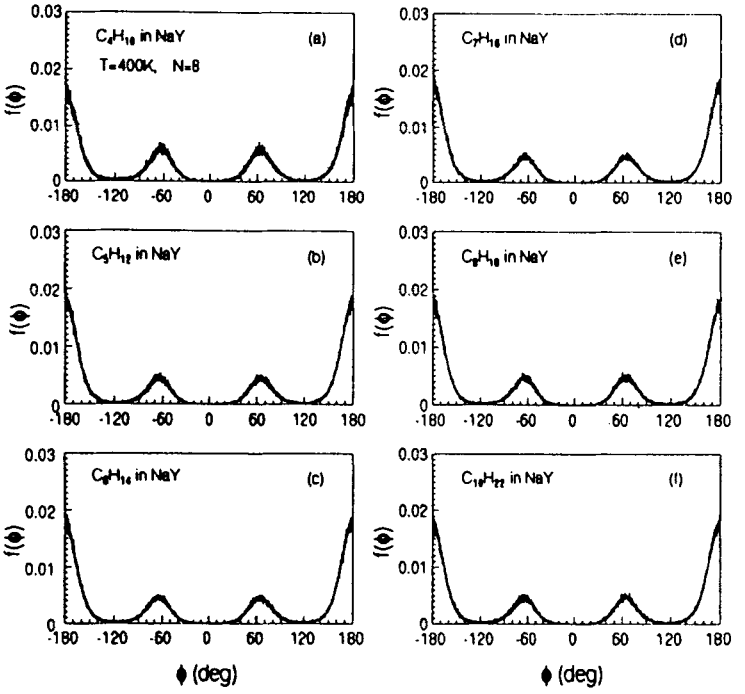

Figure 17. Dihedral angle distribution function $f(\phi)$ for n-alkanes ranging from n-butane (C_4H_{10}) to n-decane ($C_{10}H_{22}$) confined within the α-cages of zeolite NaY.

alkanes (n-hexane and n-heptane). For octane and decane in zeolite Y it is observed that the probability of the central C–C dihedral bond to be in *gauche* form is higher compared to its nearest neighbouring C–C dihedral bonds, but it is less than the probability of a terminal C–C *gauche* bond (see figure 20). For example, probability of a central *gauche* bond for n-octane confined in zeolite Y is 35·6%, which is higher than the corresponding probability for its nearest non-terminal C–C dihedral bond 2 or 2′, (32·0%), but less than that for a terminal C–C dihedral bond 3 or 3′ (39·6%) (see table 9). Similar behaviour is also observed for n-decane in Y. The probability of a *gauche* C–C dihedral bond is maximum for n-decane at one end of the chain, 4 or 4′ (38·1%). Probability of the central C–C bond to be in *gauche* form is 36·8%, which is less than that of the terminal C–C dihedral bonds (38·1%), but higher than those of the other non-terminal dihedral bonds (31·1 and 35·1%). There is some difference in the conformations of different C–C dihedral bonds for n-octane and n-decane confined in zeolite A as compared to those in zeolite Y. For octane and decane confined in zeolite A the probability of a *gauche* C–C dihedral bond is maximum at the centre of the chain rather than at the ends (see figure 21). For example, the probability of the central C–C dihedral bond to be *gauche* for n-octane confined in A is 49·7%, which is higher than the probability for both terminal (46·6%) as well as other non-terminal C–C dihedral bonds (41·0%) (see table 10). The probability of a *gauche* bond at the centre of the chain is even higher for n-decane confined in zeolite A.

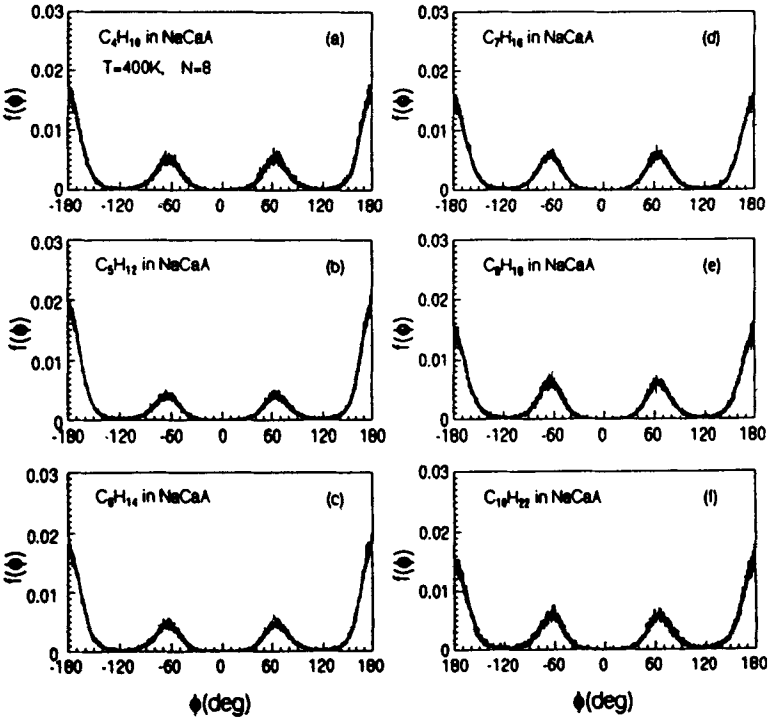

Figure 18. Dihedral angle distribution function $f(\phi)$ for n-alkanes ranging from n-butane (C_4H_{10}) to n-decane ($C_{10}H_{22}$) confined within the α-cages of zeolite NaCaA.

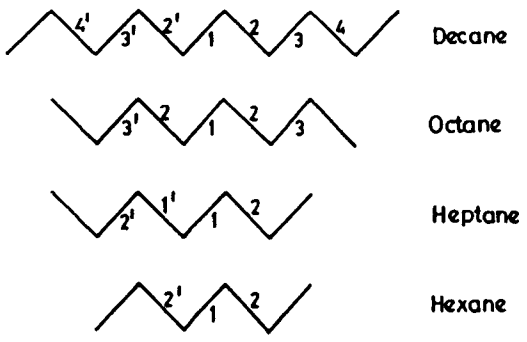

Figure 19. Schematic diagram representing the convention adopted in numbering the C–C dihedral bonds along the chain for n-hexane (C_6H_{14}) to n-decane ($C_{10}H_{22}$).

It is clear from the above discussions that for long alkanes the effect of confinement on conformational properties is more pronounced when the molecules are confined in zeolite A. It is observed that the long n-alkane molecules exhibit a significant departure from linear shape when confined in zeolite A, which is reflected in large enhancement of the probability of finding a *gauche* bond at the centre of the chain

Table 7. Average relative population of *trans* and *gauche* bonds for different *n*-alkanes (C_4H_{10} to $C_{10}H_{22}$) in zeolite NaY at a temperature of 400 K and sorbate concentration, $c = 1$ *n*-alkane/α-cage.

Molecule	*%trans*	*%gauche*
C_4H_{10}	57·0	43·0
C_5H_{12}	66·1	33·9
C_6H_{14}	65·8	34·2
C_7H_{16}	64·4	35·6
C_8H_{18}	64·3	35·7
$C_{10}H_{22}$	65·1	34·9

Table 8. Average relative population of *trans* and *gauche* bonds for different *n*-alkanes (C_4H_{10}–$C_{10}H_{22}$) in zeolite NaCaA at a temperature of 400 K and sorbate concentration, $c = 1$ *n*-alkane/α-cage.

Molecule	*%trans*	*%gauche*
C_4H_{10}	59·6	40·4
C_5H_{12}	68·4	31·6
C_6H_{14}	64·7	35·3
C_7H_{16}	57·0	43·0
C_8H_{18}	55·0	45·0
$C_{10}H_{22}$	57·6	42·4

Table 9. Percentage probability of remaining in *trans* or *gauche* form for every C–C dihedral bond along the chain for different *n*-alkanes (C_6H_{14}–$C_{10}H_{22}$) in zeolite NaY at a temperature of 400 K and sorbate concentration, $c = 1$ *n*-alkane/α-cage.

Molecule	Bond	*%trans*	*%gauche*
C_6H_{14}	1	72·4	27·6
	2 or 2′	62·5	37·5
C_7H_{16}	1 or 1′	68·5	31·5
	2 or 2′	60·2	39·8
C_8H_{18}	1	64·4	35·6
	2 or 2′	68·0	32·0
	3 or 3′	60·4	39·6
$C_{10}H_{22}$	1	63·2	36·8
	2 or 2′	64·9	35·1
	3 or 3′	68·9	31·1
	4 or 4′	61·9	38·1

Table 10. Percentage probability of remaining in *trans* or *gauche* form for every C–C dihedral bond along the chain for different *n*-alkanes (C_6H_{14}–$C_{10}H_{22}$) in zeolite NaCaA at a temperature of 400 K and sorbate concentration, $c = 1$ *n*-alkane/α-cage.

Molecule	Bond	*%trans*	*%gauche*
C_6H_{14}	1	74·5	25·5
	2 or 2′	59·9	40·1
C_7H_{16}	1 or 1′	65·1	34·9
	2 or 2′	48·8	51·2
C_8H_{18}	1	50·3	49·7
	2 or 2′	59·0	41·0
	3 or 3′	53·4	46·6
$C_{10}H_{22}$	1	41·5	58·5
	2 or 2′	51·3	48·7
	3 or 3′	65·4	34·6
	4 or 4′	64·2	35·8

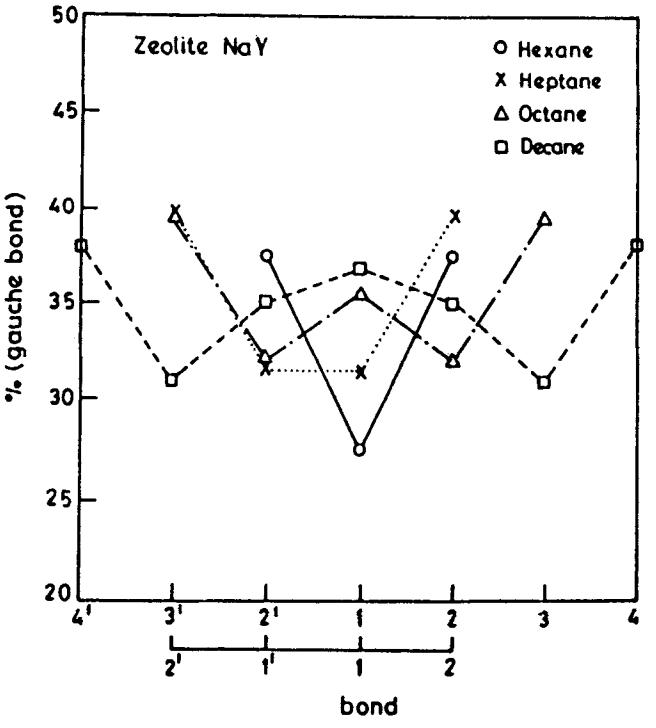

Figure 20. Percentage variation of *gauche* bonds along the chain for different *n*-alkanes (C_6H_{14} to $C_{10}H_{22}$) confined in zeolite NaY.

rather than towards the end. In figure 22 we have shown snapshots of actual conformation of an *n*-octane and *n*-decane molecule confined in zeolite Y obtained from simulations.

These figures clearly demonstrate that in zeolite Y, long *n*-alkane molecules are able to remain in stretched conformation, whereas in zeolite A, the molecules are much more coiled within the α-cage. Although the sorbate–zeolite interaction energy, U_{sz}, might play some role in determining the conformational properties of *n*-alkane molecules, but it seems to us that steric factor arising from the differences in topology of the voids in zeolites Y and A is mainly responsible for the observed differences in conformational properties of long *n*-alkanes confined in these two zeolites. The main difference between the voids in zeolites Y and A is the dimension of the windows separating two adjacent α-cages. In zeolite Y, α-cages are interconnected in a tetrahedral fashion via 12-ring windows of approximately 8 Å diameter. On the other hand, in zeolite A the α-cages are octahedrally connected through 8-ring windows of much smaller dimension, ~ 4·5 Å. Besides, the dimension of an α-cage in zeolite A is also smaller than that in zeolite Y. Because of large window diameter in zeolite Y, long *n*-alkane molecules can stretch between two α-cages quite comfortably. In figure 22b it is shown how an *n*-decane molecule during simulation can occupy two adjacent α-cages through the window connecting them. As a result, the steric influence on long *n*-alkanes within an α-cage of zeolite Y is less, and, therefore, the molecules have more freedom to remain in stretched

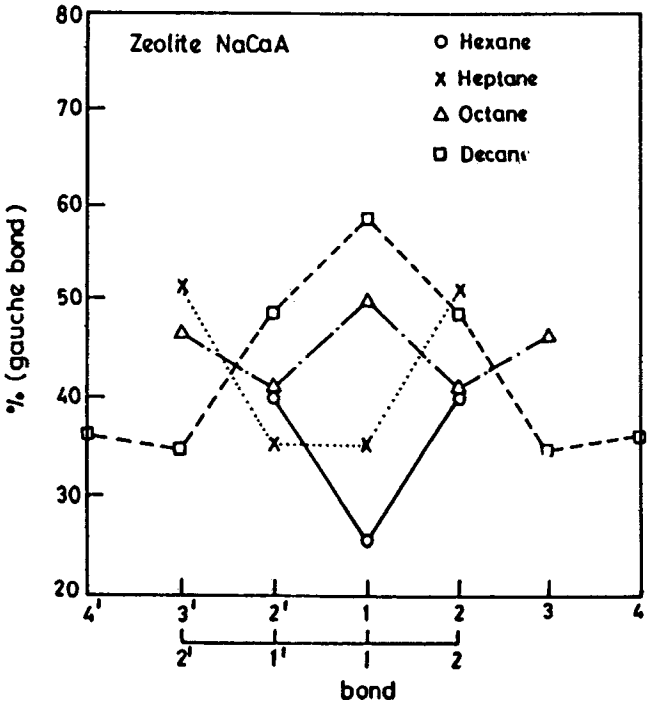

Figure 21. Percentage variation of *gauche* bonds along the chain for different *n*-alkanes (C_6H_{14} to $C_{10}H_{22}$) confined in zeolite NaCaA.

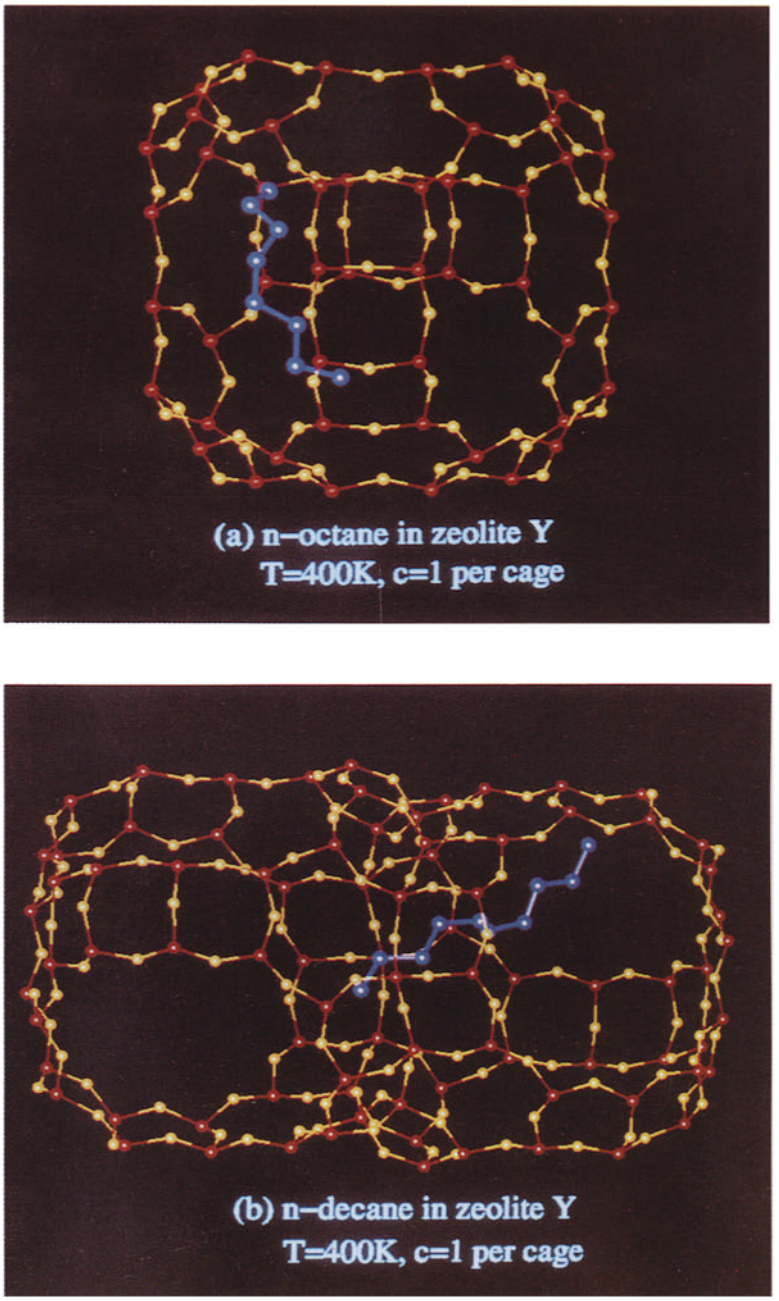

Figure 22. Snapshots of an (**a**) *n*-octane and (**b**) *n*-decane molecule confined within the α-cages of zeolite NaY obtained from the MC simulation at 400 K and $c = 1$ *n*-alkane/α-cage.

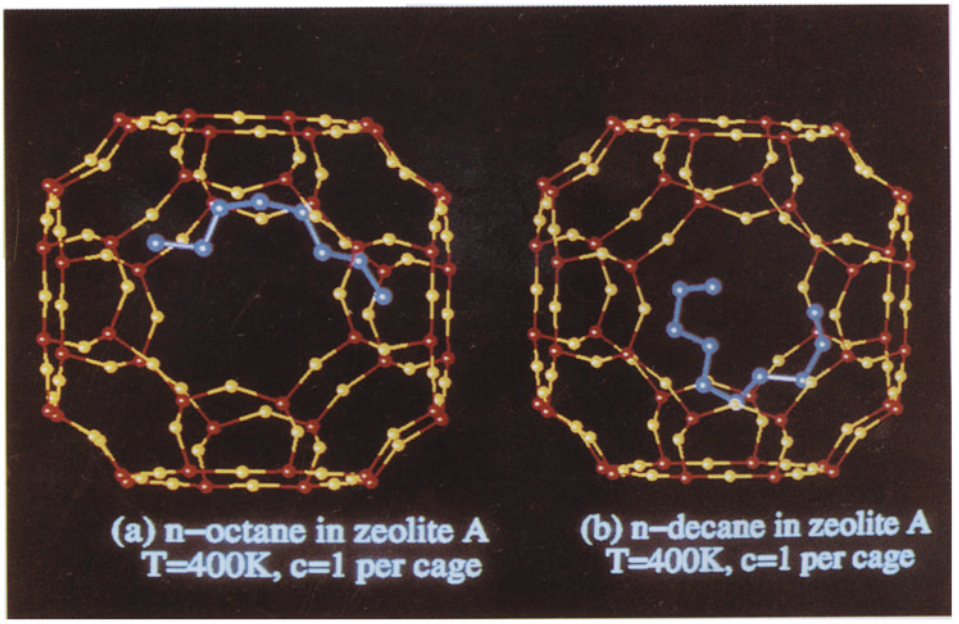

Figure 23. Snapshots of an (a) *n*-octane and (b) *n*-decane molecule confined within the α-cages of zeolite NaCaA obtained from the MC simulation at 400 K and $c = 1$ *n*-alkane/α-cage.

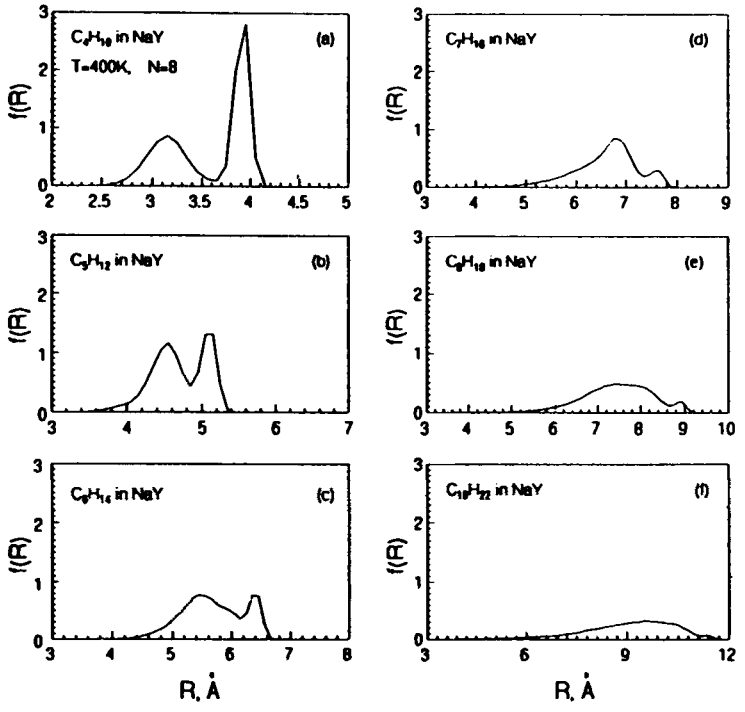

Figure 24. Distribution of end-to-end distance $f(R)$ of *n*-alkanes ranging from *n*-butane (C_4H_{10}) to *n*-decane ($C_{10}H_{22}$) confined within the α-cages of zeolite NaY.

conformation. On the other hand, due to smaller window dimension in zeolite A, long *n*-alkane molecules find it difficult to migrate or stretch through the windows. Therefore, the molecules remain mostly confined in an α-cage. As a result, as the chain length increases the *n*-alkanes assume more and more coiled conformation with very large population of central C–C *gauche* bond (see figure 23). Note that this type of confinement within the α-cage of zeolite A is also observed for small chain such as *n*-butane at different concentrations and temperatures (Bandyopadhyay and Yashonath 1997).

Figures 24 and 25 show the distribution of end-to-end distance $f(R)$ of different *n*-alkane molecules starting from *n*-butane to *n*-decane in zeolites Y and A respectively.

End-to-end distance (R) of an *n*-alkane molecule with chain length M is calculated as the distance between the first and the Mth methyl groups (i.e. the two end methyl groups in a chain). This distribution gives an estimation of the change in conformations of *n*-alkane molecules with increase in chain length. The distribution for *n*-butane ($M=4$) in both zeolites Y and A consists of two peaks. A sharp peak of high intensity is observed at an end-to-end distance $R \sim 3{\cdot}9$ Å, which corresponds to *trans* *n*-butane. A broad peak, with much lower intensity, is observed around $R=3{\cdot}1$ Å, which corresponds to the *gauche* *n*-butane. In both zeolites Y and A as the alkane chain length is increased intensity of the peak, corresponding to the *trans* conformation, decreases and that corresponding to the *gauche* conformation increases. In zeolite Y, up to $M=8$, the curves consist of two peaks, which suggest

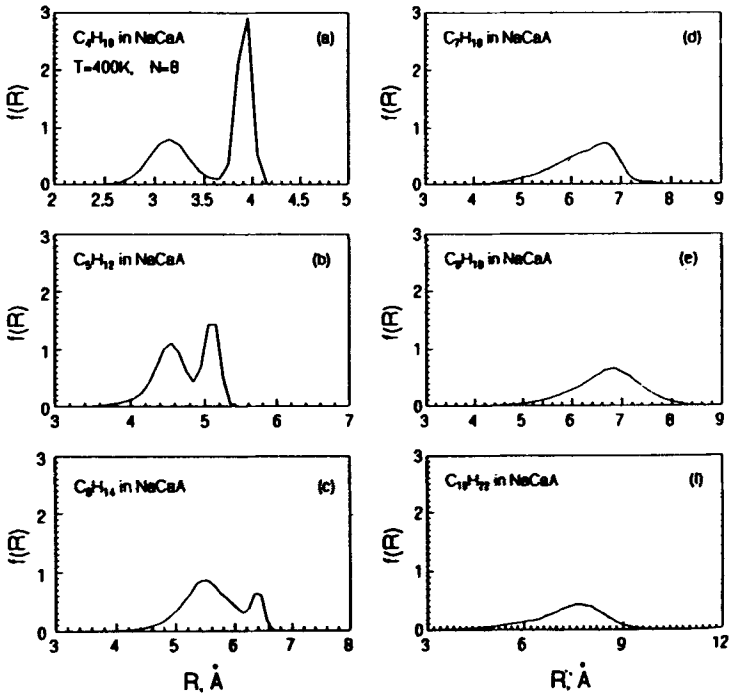

Figure 25. Distribution of end-to-end distance $f(R)$ of *n*-alkanes ranging from *n*-butane (C_4H_{10}) to *n*-decane ($C_{10}H_{22}$) confined within the α-cages of zeolite NaCaA.

that although population of *gauche* bonds has increased but still the molecules remain in stretched conformation. In zeolite A, for $M \geq 7$, the distribution becomes unimodal and the peak appears at much lower value of R compared to that observed in zeolite Y. For example, for *n*-decane in zeolite A, the peak in the distribution is at 7·5 Å whereas in zeolite Y, the maxima in the peak appears around 10 Å. In fact distribution is almost zero in zeolite A for $R > 9$ Å. Similar trend is also observed for *n*-heptane and *n*-octane. This shift of maxima towards lower values of R for long *n*-alkanes ($M \geq 7$) confined in zeolite A, proves that conformations of these molecules deviate significantly from linear shape, which is a consequence of large enhancement of central *gauche* bonds.

4. Conclusions

It is seen that the geometry and the energy of the clusters confined in zeolite NaCaA are strongly influenced by the symmetry of the cavity in which it is confined. A plot of the $\Delta U/\Delta n$ for various n for the confined clusters suggests the existence of magic numbers among confined clusters. The magic numbers for the confined clusters are different from those encountered for free clusters. This is the first time that evidence for the possible existence of magic numbers for the confined clusters has been obtained. It is, however, necessary to carry out a more thorough search to ensure that the global minimum has been obtained for every cluster size. Variation of the melting temperature with n and other relevant properties will be helpful to decide about the existence or otherwise of the magic numbers.

Simulated annealing is a method employed widely to perform global optimization of complex systems. In this method, the system is cooled slowly and it is hoped that the system reached the global minimum. In the present work, we have chosen to start with any arbitrary configuration and slowly increase the temperature. As the temperature is increased the system begins to sample the phase space more efficiently, and it is found that at some temperature the system falls from the local minimum into the global minimum or an energy close to it. It is necessary to explore this method for other complex problems such as the travelling salesman, etc.

We have compared the conformational behaviour of long *n*-alkanes confined in zeolites NaY and NaCaA. It appears that conformational properties of *n*-alkanes in zeolite A are significantly different from those in zeolite Y. This difference is more pronounced for $M \geq 8$. It is observed that up to $M = 7$, probability of a central *gauche* bond is less than that of the terminal C–C dihedral bonds in both zeolites Y and A. But in zeolite A for $M \geq 8$, it is observed that probability of a central *gauche* bond is highest among all the C–C dihedral bonds. This shows that in zeolite A, long *n*-alkane molecules deviate significantly from linear conformation. This effect is much less pronounced in zeolite Y. We attribute this difference in conformational properties in zeolites Y and A to the difference in the dimension of the windows connecting two α-cages. In zeolite Y windows are of much wider dimension (8 Å diameter), compared to those in zeolite A (4·5 Å diameter). As a result of large window diameter a long *n*-alkane molecule can easily migrate between the α-cages as well as can stretch itself within two α-cages through the window, and therefore can remain in a conformation not much different from a

linear one. But narrow windows present in zeolite A do not allow a long-chain molecule to pass through it. As a result, the molecules mostly remain coiled within an α-cage of zeolite A. Large increase in sorbate–zeolite interaction energy in zeolite A with increase in chain length also influences the conformational properties of long n-alkane molecules. Shift of the maxima in end-to-end distance distribution towards lower value of R for long n-alkanes confined in zeolite A also suggests significant deviation of the molecules from linear shape.

References

Adams J E and Stratt R M 1990a *J. Chem. Phys.* **93** 1332
Adams J E and Stratt R M 1990b *J. Chem. Phys.* **93** 1358
Adams J E and Stratt R M 1990c *J. Chem. Phys.* **93** 1632
Allen M P and Tildesley D J 1987 *Computer simulation of liquids* (Oxford: Clarendon Press)
Bandyopadhyay S and Yashonath S 1997 *J. Phys. Chem.* (communicated)
Beck T L and Marchioro II T L 1990 *J. Chem. Phys.* **93** 1347
Berry R S 1994 *J. Phys. Chem.* **98** 6910
Berry R S and Cheng H-P 1992 *Physics and chemistry of finite systems: From clusters to crystals* (Kluwer Academic Pub.) Vol. I, p. 277
Chitra R and Yashonath S 1997 *J. Phys. Chem.* **B101** 389
Cheng H-P and Berry R S 1992 *Phys. Rev.* **A45** 7969
Chmelka B F, Raftery D, McCormick A V, de Menorval L C, Levine R D and Pines A 1991 *Phys. Rev. Lett.* **66** 580
Davis H L, Jellinek J and Berry R S 1987 *J. Chem. Phys.* **86** 6456
Etters R D and Kaelberer J 1977 *J. Chem. Phys.* **66** 5112
Fitch A N, Jobic H and Renouprez A 1986 *J. Phys. Chem.* **90** 1311
Frantz D D 1995 *J. Chem. Phys.* **102** 3747
Frenkel D, Mooij G C A M and Smit B 1992 *J. Phys.: Condens. Matter* **4** 3053
Harris J and Rice S A 1988 *J. Chem. Phys.* **88** 1298
Heink W, Karger J, Pfeifer H, Salverda P, Datema K P and Nowak A 1992 *J. Chem. Soc. Faraday Trans.* **88** 515
Henson N J, Cheetham A K, Peterson B K, Pickett S D and Thomas J M 1993 *J. Computer-Aided Mater. Design* **1** 41
Hernandez E and Catlow C R A 1995 *Proc. R. Soc. London* **A448** 143
Hoare M R and Pal P 1970 *Nature* **230** 5
Honeycutt J D and Andersen H C 1987 *J. Phys. Chem.* **91** 4950
Inglesfield E J 1982 in *Computer simulation of solids* (eds) C R A Catlow and W C Mackrodt (Berlin: Springer Verlag)
Jorgensen W L, Madura J D and Swenson C J 1984 *J. Am. Chem. Soc.* **106** 6638
June R L, Bell A T and Theodorou D N 1990 *J. Phys. Chem.* **94** 1508
June R L, Bell A T and Theodorou D N 1992 *J. Phys. Chem.* **96** 1051
Karger J and Ruthven D M 1992 *Diffusion in zeolites and other microporous solids* (New York: John Wiley & Sons)
Karger J, Pfeifer H, Rauscher M and Walter A 1980 *J. Chem. Soc. Faraday Trans. I* **76** 717
Kirkpatrick K S, Gelatt C D and Vecchi M P 1983 *Science* **220** 671
Kiselev A V and Du P Q 1981 *J. Chem. Soc. Faraday Trans. II* **77** 1
Kunz R E and Berry R S 1993 *Phys. Rev. Lett.* **71** 3987
Laso M, de Pablo J J and Suter U W 1992 *J. Chem. Phys.* **96** 2817
Li F-Y and Berry R S 1995a *J. Phys. Chem.* **99** 2459
Li F-Y and Berry R S 1995b *J. Phys. Chem.* **99** 15557
Maginn E J, Bell A T and Theodorou D N 1995 *J. Phys. Chem.* **99** 2057
Metropolis N, Rosenbluth A, Rosenbluth M, Teller A and Teller E 1953 *J. Chem. Phys.* **21** 1087
Mooij G C A M, Frenkel D and Smit B 1992 *J. Phys: Condens. Matter* **4** L255
Nauchitel V V and Pertsin A J 1980 *Mol. Phys.* **40** 1341
de Pablo J J, Laso M and Suter U W 1992 *J. Chem. Phys.* **96** 6157

de Pablo J J, Laso M, Suter U W and Cochran H D 1993 *Fluid Phase Equilib.* **83** 323
Pluth J J and Smith J V 1980 *J. Am. Chem. Soc.* **102** 4704
Quirke N and Sheng P 1984 *Chem. Phys. Lett.* **110** 63
Richards R E and Rees L V C 1987 *Langmuir* **3** 335
Rosenbluth M N and Rosenbluth A W 1955 *J. Chem. Phys.* **23** 356
Santikary P, Yashonath S and Ananthakrishna G 1992 *J. Phys. Chem.* **96** 10469
Seeley G and Keyes T 1989 *J. Chem. Phys.* **91** 5581
Siepmann J I and Frenkel D 1992 *Mol. Phys.* **75** 59
Siepmann J I, Karaborni S and Smit B 1993a *Nature* **365** 330
Siepmann J I, Karaborni S and Smit B 1993b *J. Am. Chem. Soc.* **115** 6454
Smit B and Siepmann J I 1994a *J. Phys. Chem.* **98** 8442
Smit B and Siepmann J I 1994b *Science* **264** 1118
Thamm H 1987 *Zeolites* **7** 341
Van der Ploeg P and Berendsen H J C 1982 *J. Chem. Phys.* **76** 3271
Wright P A, Thomas J M, Cheetham A K and Nowak A K 1985 *Nature* **318** 611